journal

J. Am. Ceram. Soc., 95 [9] 2746–2752 (2012)
DOI: 10.1111/j.1551-2916.2011.05029.x
© 2011 The American Ceramic Society

Nanocomposite Ti–Si–N Coatings Deposited by Reactive dc Magnetron Sputtering for Biomedical Applications

Subramanian Balasubramanian,[‡,§,†] Ananthakumar Ramadoss,[‡] Akira Kobayashi,[§] and Jayachandran Muthirulandi[‡]

[‡]Electrochemical Materials Science Division, CSIR-Central Electrochemical Research Institute, Karaikudi 630006, India

[§]Joining and Welding Research Institute, Osaka University, Osaka 560-0047, Japan

Nanocomposite Ti–Si–N coatings were prepared by reactive dc magnetron sputtering in a mixture of Ar and N_2 gases onto bio implantable 316L stainless steel substrates. X-ray diffraction analysis revealed that the Ti–Si–N nanocomposite coatings are mainly composed of amorphous Si_3N_4 and TiN crystals. The presence of different phases like TiN, TiO_2, and Si_3N_4 was confirmed from X-ray photoelectron spectroscopy analysis. Raman spectra of the as-deposited composite coatings exhibited characteristic peaks at 207.5, 305.8, 442.5, and 571.8 cm^{-1}. HRTEM indicated columnar microstructure. A higher hardness value of 35 GPa for the nanocomposite coatings was observed. The potentiodynamic polarization and electrochemical impedance spectroscopy measurements showed that the Ti–Si–N nanocomposite coatings exhibited superior corrosion resistance compared with the Si_3N_4, TiN single layer, and the bare substrate in simulated body fluid solution.

I. Introduction

Metallic materials such as AISI 316L stainless steel, Co-Cr alloy, Ti, and Ti alloy are used as biomaterials due to their excellent mechanical and corrosion-resistant properties.[1] Most implanted metallic biomaterials have a tendency to lose electrons in solution and, as a result, they show a high potential to corrode in the biological environments, which usually cause inflammatory and loosening of the implants.[2] In addition, their low surface hardness, high friction coefficient, and poor wear resistance are also limiting their application of metallic biomaterials.[3] To protect and enhance the metallic implants from wear and corrosion and to improve their biocompatibility, tremendous surface modification techniques and coatings deposition have been applied to deposit a variety of functional coatings on the surfaces of metallic implants.

Highly sophisticated surface-related properties, such as superplasticity, optical, magnetic, electronic, and catalytic properties, can be obtained by advanced nanostructured coatings, making them attractive for industrial applications in high speed machining, tooling, biomedical, automotive, optical applications, and magnetic storage devices.[4,5] Ternary systems of (Ti, *X*) N, where *X* = B, C, Al, Si, Cr, etc. have been attractive for advanced hard coating materials[6,7] because of their superior properties, in particular, higher hardness, and improved oxidation resistance compared with TiN coatings. These coatings were characterized as being a nanocomposite, consisting of nano-sized TiN crystallites surrounded by an amorphous matrix of Si_3N_4.[8] Such nanocomposite hard coatings often display extremely higher hardness (called superhard) compared with any other ternary (Ti, *X*) N systems.[9] When Si is introduced to TiN, the hardness increases and the grain size decreases dramatically. This trend continues with progressively increasing Si additions until the hardness reaches a maximum (e.g., ~5 at.% Si), after which it drops off considerably as further Si is added.[10] The grain size decreases up to this hardness maximum, beyond which it levels off as the Si content further increases. Nanocomposite materials have been prepared using PACVD, ion-assisted ion beam sputtering, vacuum arc deposition, magnetron sputtering and recently, by hybrid arc and magnetron sputter processing.[11–15] Due to the use of toxic gas for metal sources and high substrate temperature in CVD, physical vapor deposition (PVD) technique is considered more suitable for industrial-scale synthesis of these coatings.[16] The main PVD methods are cathodic arc and magnetron sputtering. Usually, in the cathodic arc deposition process, an expensive Ti–Si compound target is necessary to deposit the Ti–Si–N composite coatings, and it is not much suitable for industrial production. The magnetron sputtering has been extensively used because of its low level of liquid–particle ejection and material consumption.

In this work, Ti–Si–N coatings were deposited onto 316L stainless steel substrates using a reactive dc magnetron sputtering technique with separate Ti and Si targets. Structural, mechanical properties of the Ti–Si–N nanocomposite coatings and their electrochemical corrosion resistance in simulated body fluid are reported in this article.

II. Experimental Procedure

Titanium silicon nitride (Ti–Si–N) coatings were deposited by reactive dc magnetron sputtering, using separate Ti (99.99%) and Si (99.99%) targets. The target power was typically set at 150 W for Ti and 100 W for Si. The base pressure of the deposition chamber was 10^{-6} torr, and the depositions were carried out with a sputtering pressure of 5×10^{-3} torr in the gaseous mixture of Ar/N_2 (50:50): both the gases were of 5 N purity. The phase composition, texture, and crystalline structure were determined using a conventional X'Pert Philips diffractometer (Eindhoven, The Netherlands). The surface morphology of the coatings was observed by Nano Navi atomic force microscopy (AFM) in tapping mode. Coating thickness was measured by profilometry using a step on a masked substrate and it was found to be about 2.2 μm. The specimen was mounted on a semiconductor support grid, which was further fabricated in a Hitachi FB-2000 (Ibaraki, Japan). Tungsten layer was coated to protect the specimen from being sputtered out by Ga ions. Two trenches were milled away in such a way that a thin

A. Bandyopadhyay—contributing editor

Manuscript No. 30227. Received September 13, 2011; approved November 21, 2011.

Paper Presented at Bangalore INDIA BIO 2011 Conference.

[†]Author to whom correspondence should be addressed. e-mail: bsmanian@cecri.res.in.

wall is left behind between the two trenches, the wall being thin enough to be electron-transparent when tilted by 90°. The specimens prepared were examined using a JEOL-JSM-2100F field emission electron microscope (Tokyo, Japan) for TEM-selected area electron diffraction (SAED) analysis. X-ray photoelectron spectroscopy (XPS; Multi Lab 2000; Thermo Scientific, The Netherlands) was employed to analyze the chemical bonding. It was performed with 5 kV Ar ions to sputter the oxide layer and survey the element signal. To investigate the carbon bonds, Raman spectroscopy measurements were undertaken on a Renishaw Ramascope 2000 spectrometer with a HeNe 632 nm laser. Coating hardness, *H*, was measured with nanoindentation (Nanotest 600; Micro Materials Ltd., Wrexham, UK, fitted with Berkovich indenter: a three-sided pyramid with the same area-to-depth ratio as a Vickers indenter). The intrinsic mechanical properties of these coatings were measured at indentation depths between 200 and 330 nm, which is less than 10% of the coating thickness, and averaging over a total of five indents. The influence of the mechanical properties of the substrate on the measurement is therefore avoided.

(1) Electrochemical Characterization

The electrochemical measurements were carried out on the samples with open circuit potential (OCP)–time measurements, potentiodynamic polarization, and electrochemical impedance spectroscopic studies, using a conventional three-electrode cell connected with a potentiostat (Autolab PGSTAT galvanostat/potentiostat). The test electrolytes for electrochemical investigations were conventional simulated body solutions prepared at pH value of 7.4.[17]

A saturated calomel reference electrode (SCE) and a platinum counter electrode were employed. The sample surface was cleaned by distilled water. Deaerated conditions under N_2 gas purging and a temperature of 37°C were used for *in vitro* experiments. The exposed surface area of all specimens was fixed at 1 cm^2 and the remaining portion except for the exposed area was painted with a strong adhesive silicon bond to prevent the initiation of crevice corrosion.

To establish the OCP, prior to the polarization measurements, the samples were immersed in the solution for about 60 min. The applied alternating potential had root mean square amplitude of 10 mV on the OCP. After getting the stable OCP, the upper and lower potential limits of linear sweep voltammetry were set at +200 and −200 mV, respectively with reference to OCP. The sweep rate was 1 mV/s. The corrosion potential E_{corr}, corrosion current I_{corr} and corrosion rate were determined by the Tafel extrapolation method. Impedance measurements were conducted using a frequency response analyzer and the spectrum was recorded in the frequency range of 10 mHz–100 kHz.

III. Results and Discussion

(1) Compositional Analysis

XPS analysis was employed to acquire information on chemical structure and bonding states in the Ti–Si–N nanocomposite coatings. Prior to the XPS measurements, coatings were sputter cleaned by 500 eV Ar^+ etching for 1 min to remove the surface contaminants. XPS survey spectrum of the Ti–Si–N nanocomposite coatings is shown in Fig. 1(a). The coatings exhibit the characteristic Ti2p, Si2p, N1s, O1s, and C1s peaks at the corresponding binding energies 458.7, 101.5, 396.3, 531.7, and 283.8 eV, respectively.[18] The peak deconvolution reveals the presence of different binding states for Ti, Si, N, O, as well as for C. Typical, XPS core-level spectra of the coatings were fitted using the Gaussian and Lorentzian profile. In these experiments, a linear-type background-subtraction was used.

The deconvolution Ti2p spectra [Fig. 1(b)] could be fitted well with five components. The peaks observed at 455.8 and 460.9 eV are attributed to the Ti2p3/2 and Ti2p1/2 electron binding energy of the TiN phase, and are in agreement with the previous reports.[19] The chemical shifts in the core level of the TiN layer relative to elemental Ti reflect a charge transfer from titanium to nitrogen during the nitridation process. The higher position peak observed at 458.5 eV is attributed to the Ti2p3/2 electron binding energy of the TiO_2 phase. The peak at 462.7 eV is assigned to chemical bonds of TiO_xN_y phase. The peak at 464.3 eV can be attributed to TiO_2 (oxide).[19]

The XPS spectrum of Si2p of nanocomposite coating is shown in Fig. 1(c). The main characteristic peak locates at the binding energy of 101.5 eV corresponding to the Si_3N_4 formation.[20] The other peak at 102.4 eV comes from the Si2p electrons in SiO_2. The N1s spectrum of the nanocomposite coatings [Fig. 1(d)] shows the typical characteristic of nitride TiN and Si_3N_4 coatings with binding energies at around 396.2 and 397.0 eV, respectively.[21] The broad N1s spectra [Fig. 1(d)] of the Ti–Si–N coatings obviously indicate the presence of both TiN and Si_3N_4. It appears that the amount of N in nanocomposite coatings is mainly in the form of TiN with relatively small amounts of Si_3N_4.

Deconvolution of the O1s region shows six components in the as-inserted sample [Fig. 1(e)]. Two of them, at 529.9 and 530.7 eV, are quite well known, and show the existence of TiO_2 and SiO_2 phase. The peaks at 531.6 and 532.3 eV could be assigned to hydroxyl groups (OH^-).[22] Finally, to obtain a good fit of the O 1s line, it is necessary to introduce a contribution at binding energy values of 533.1 and 534.4 eV, which are usually attributed to H_2O bonds.[23] The deconvoluted C1s spectrum of as-deposited Ti–Si–N coatings [Fig. 1(f)] shows peaks at 286.2, 287.1, and 289.9 eV, which are assigned to C–O, C–N and C = O, respectively.[24]

The high amount of adventitious carbon, despite the high vacuum during the XPS measurements, suggests that carbon was deposited on the coating surface during the deposition process or sample storage.[25] Furthermore, carbon and oxygen incorporation might have occurred due to the air contamination when the films were transferred from the sputtering instrument to the XPS sample chamber.

Raman microscopy is to elucidate the behavior of the optic and acoustic phonon modes of the (cubic) crystalline lattices. The phonon bands of Ti–Si–N that have attributed the scattering in the acoustic range are determined by the vibrations of the heavy Ti ions (typically 150–300 cm^{-1}) and in the optic range by the vibrations of the lighter N ions (typically 400–650 cm^{-1}). The characteristic peaks at 207.5, 305.8, 442.5, and 571.8 cm^{-1}, related to transverse acoustic (TA)/longitudinal acoustic (LA), second-order acoustic (2A) modes of TiN, respectively, were observed in the Raman spectra of Ti–Si–N coatings (Fig. 2) prepared by reactive sputtering process. This is in good agreement with the reported values for Ti–Si–N coatings.[26]

(2) Structural and Microstructural Analysis

The X-ray diffraction (XRD) spectrum of TiN single layer coating is shown in Fig. 3. The coatings were found to be crystallized in cubic structure with preferential orientation along (200) plane. The XRD pattern of single phase Si_3N_4 coating showed no peaks, indicating its amorphous nature. The pattern shows only diffraction peaks due to crystalline TiN, with no indication of the presence of crystalline Si_3N_4 phases, suggesting that Si is present in amorphous state. The observed *d* values are in good agreement with the standard values with JCPDS card no 087-0633 for TiN coatings. XRD patterns revealed the presence of only one phase that can be assigned to the cubic B1 NaCl structure, typical for TiN, and the peaks corresponding to (111), (200), (220), (311), and (400) planes were observed. The pattern shows only diffraction peaks with a TiN (2 0 0)-preferred orientation. It is probably a solid solution (Ti, Si) N by a substitution of Si

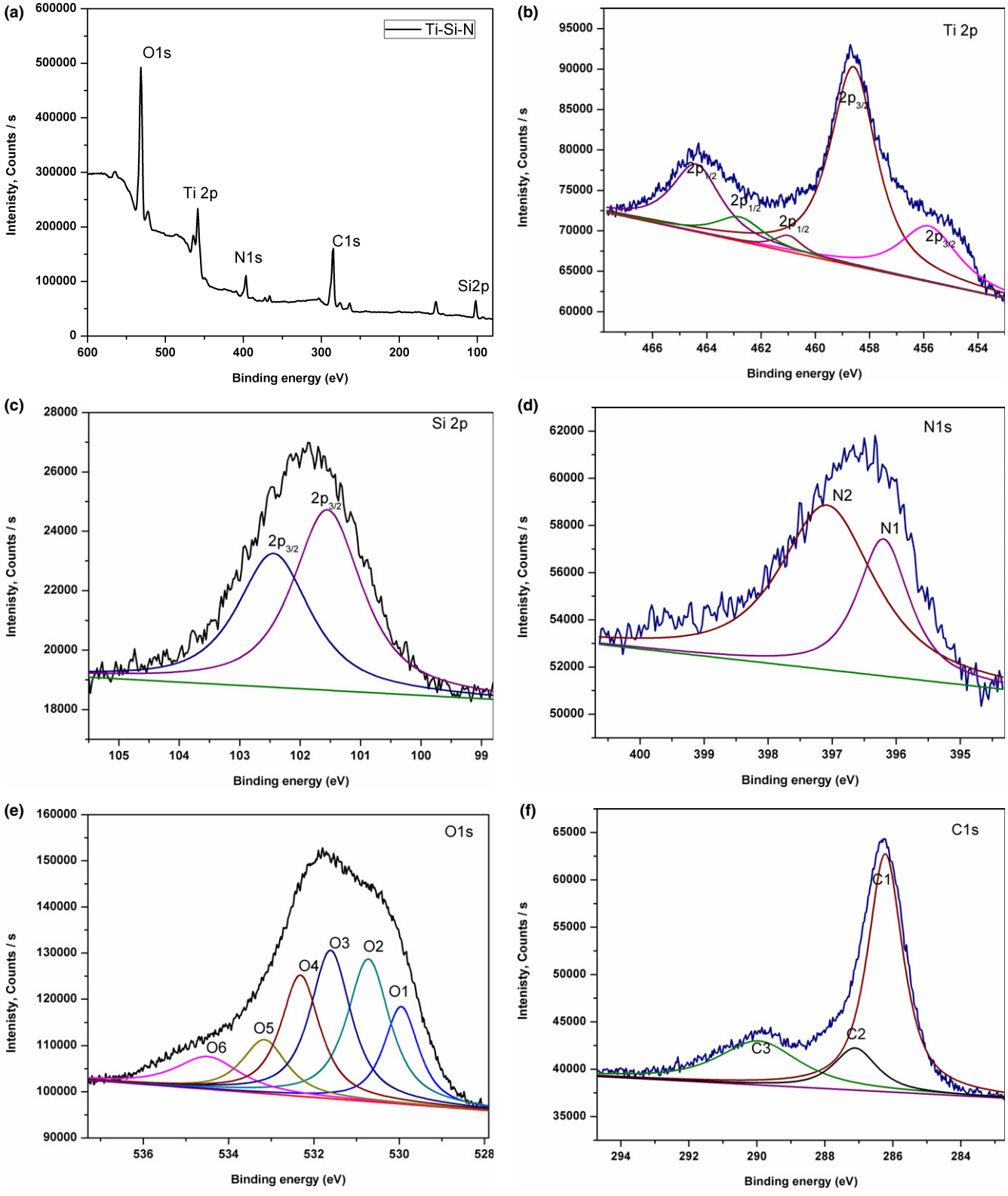

Fig. 1. Survey spectra of the Ti–Si–N coatings (a) Survey, (b) Ti2p, (c) Si2p, (d) N1s, (e) O1s, and (f) C1s.

for Ti in TiN lattice, because the ionic radius of Si^{4+} ion (0.041 nm) is smaller than that of Ti^{3+} (0.075 nm) ion. The average grain size value was calculated to be about 30–40 nm. The grain size reductions to the nanometer range result in considerable improvement in their resistance to localized corrosion.[27]

The surface topography of the Ti–Si–N coatings was studied using AFM. The basic study comprised 3D representations for a scanned area of 2 μm × 2 μm, which are shown in Fig. 4. Ti–Si–N nanocomposite layer had much smooth surface. The roughness (RMS) value, estimated from these images, was 3.7 nm. The surface roughness of these sputtered Ti–Si–N films is much smoother compared with those prepared by inductively coupled plasma,[28] which has surface roughness between 18 and 23 nm.

The layer morphology and crystal phase of the Ti–Si–N coatings are analyzed from cross-section analysis with HRTEM as shown in Fig. 5(a). Distinct interfaces can be seen at the boundaries between the glass substrate and the first layer being deposited. The micrograph suggests that

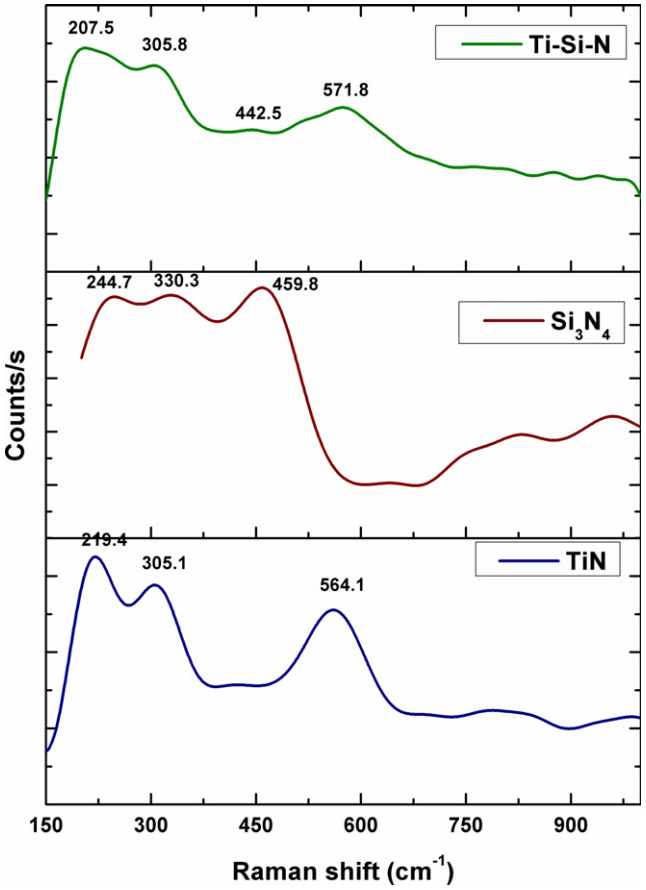

Fig. 2. X-ray diffraction spectra of nanocomposite coatings (a) TiN, (b) Si_3N_4, and (c) Ti–Si–N.

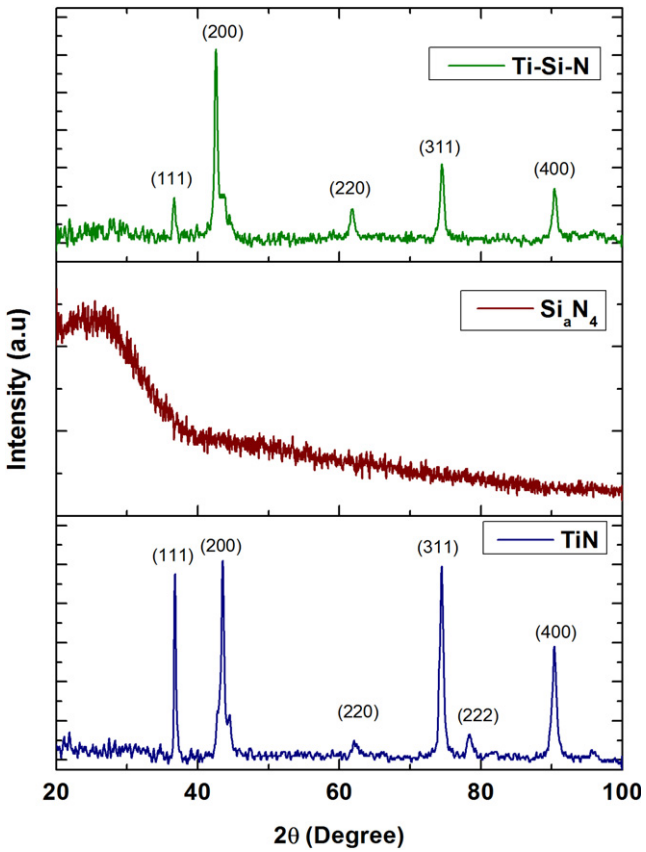

Fig. 3. Laser Raman spectra of nanocomposite coatings (a) TiN, (b) Si_3N_4, and (c) Ti–Si–N.

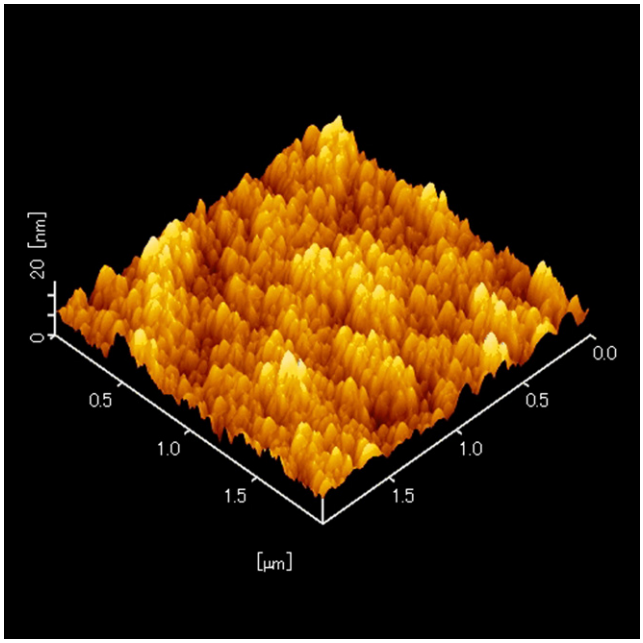

Fig. 4. A representative AFM image of surface of Ti–Si–N nanocomposite coating.

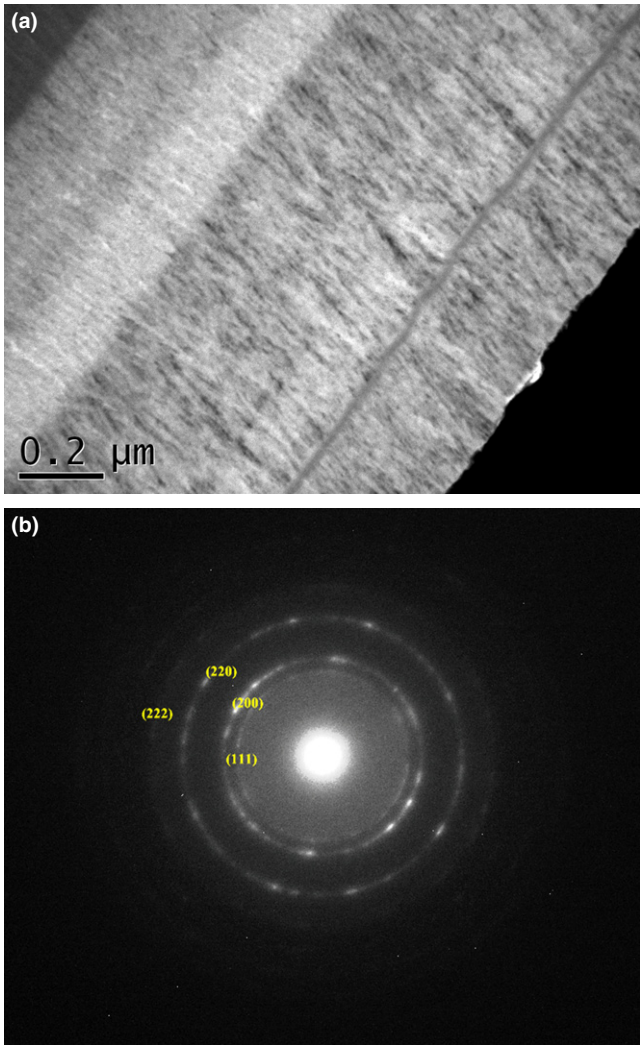

Fig. 5. (a) HRTEM image pattern of Ti–Si–N nanocomposite coating. (b) SAED pattern of Ti–Si–N nanocomposite coating.

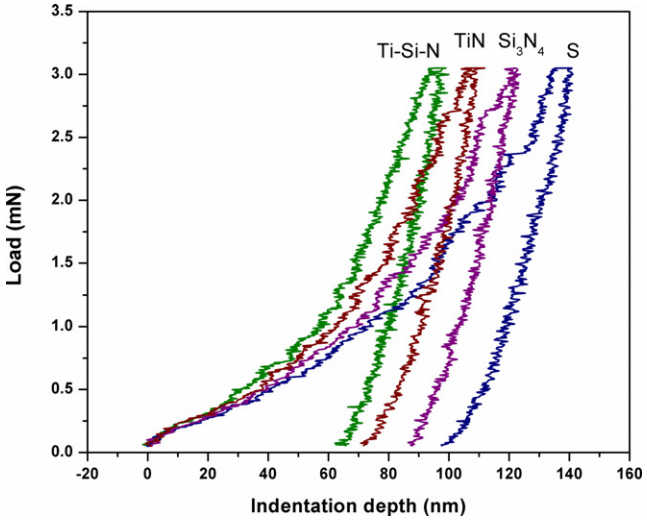

Fig. 6. Typical load vs. displacement curves for 316LSS, Si_3N_4, TiN, and Ti–Si–N nanocomposite coatings at 3 n*M* load.

the appearance of the Si_3N_4 layer is darker compared with the lighter contrast of the TiN layer. This is because of the higher atomic number of Si_3N_4 layers.[29]

The microstructure of Ti–Si–N composite layer consists of columnar grains with an average of width of 50–100 nm. They are oriented in such a way that the longer axes of the grains are parallel to the growth direction of the coating. An evident dense structure by deposition of TiN and Si_3N_4 layers is again verified, which is consistent with AFM results. The layered structure is pronounced due to the immiscibility of TiN and Si_3N_4 layers. The columnar microstructure is typical of the coatings deposited at low temperature and low gas pressure in sputtering process. The sample did not display any inter-lamella cracking indicating good adhesion. The SAED patterns as shown in Fig. 5(b) indicate that the nanocomposite coatings have polycrystalline structures with a randomly oriented cubic δ-TiN (NaCl-type structure). There is no indication of rings corresponding to Si_3N_4, indicating the solid solution nature of (Ti Si)N, which is in corroboration with the XRD results.

(3) Nanohardness

Figure 6 compares the load–indentation depth curves of the steel substrate, single-layer TiN, Si_3N_4, as well as Ti–Si–N nanocomposite coatings. The indentation depth at a maximum load of 3 mN decreases from 140 nm for the 316L SS substrate to 80 nm for Ti–Si–N nanocomposite coatings. The hardness of the 316L SS substrate was approximately 15 GPa. The indenter penetration depth of the Si_3N_4 single layer was approximately 110 nm at a hardness of approximately 21 GPa. When compared, the penetration depth in the TiN layer was approximately 93 nm and the hardness was 25 GPa, whereas in the Ti–Si–N nanocomposite coatings, the penetration depth was approximately 81 nm and the hardness was 39 GPa. The hard coating layer formed on the steel surface increases the hardness. In particular, Ti–Si–N coatings showed considerably enhanced hardness, which could be attributed to the crystal size refinement due to the incorporation of Si in accordance with the Hall–Petch relationship.[30,31] A strong tendency of decreasing intensity and broadening of the width of the TiN (111) peak was also observed, indicating the diminution of the grain size or the residual stress induced in the crystal lattice.[32] It could be confirmed that the Si incorporation reduced the crystal size and the residual stress and hence higher hardness observed for these coatings.

(4) Corrosion Studies in Simulated Body Fluid

Implant materials used inside the human body are generally exposed to an aqueous environment containing various anions (Cl^-, HCO_3^-, HPO_4^{2-}), cations (Na^+, K^+, Ca^{2+}, Mg^{2+}), organic substances, and dissolved oxygen.[33] Hence, metallic implant materials are prone to aqueous corrosion. The metallic components of the alloy are initially oxidized to their ionic forms, and release a free electron. The dissolved oxygen present in the aqueous environment will react with the water molecules and free electron to form hydroxyl ions. These hydroxyl anions react with the metallic cations to form a corrosion product. During the corrosion process, both the anodic and cathodic reactions must proceed in balance to maintain the overall electrical neutrality. Electrochemical impedance spectroscopy (EIS) is a powerful technique to study the electrochemical properties of the PVD coating system due to its high sensitivity to the coating structure. The results of corrosion testing for the substrate, TiN, Si_3N_4, and Ti–Si–N coatings are given in Table I. The Bode and Nyquist plots in Figs. 7 and 8 respectively show the EIS spectra of coatings at open-circuit potential during immersion in SBF solution. When the sample is immersed in the electrolyte, the defects in the coating provide the direct diffusion path for the corrosive media. In this process, the galvanic corrosion cells are formed, and localized corrosion dominates the corrosion process. The electrochemical interface can be divided into two sub-interfaces: electrolyte/coating and electrolyte/substrate. The single semicircle behavior obtained for the samples is believed to be due to the short exposure time (60 min), which is not sufficient to reveal the degradation of the substrate.[34] The R_{ct} increases in the following order: Substrate < TiN < Si_3N_4 < Ti–Si–N.

For the nanocomposite coatings, the Ti–Si–N layers were deposited wherein the growth of the columnar structure of the individual TiN layer, which is detrimental to coatings used in severe corrosion environments, was suppressed markedly. Therefore, the formation of through-pinhole coating channels is eliminated, which means that the possibility of the corrosive solution contacting the substrate is highly reduced. Amorphous coatings like *a*-Si_3N_4, *a*-BN_x, *a*-C, exhibit high corrosion resistance because of their dielectric nature and dense microstructure without preferential corrosion paths like grain boundaries and other structural defects. For the sputtered coatings, the dense microstructure and reduced crystallite size of the nanocomposite coatings are attributed to the ion bombardment during deposition and incorporation of the amorphous phase in the nanocrystalline matrix, and the poor electrical conductivity of the amorphous constituent in the nanocomposite coating (e.g., Si_3N_4 in TiN/Si_3N_4 nanocomposites). The comparative study of the impedance spectra of the specimens elicited that the Ti–Si–N nanocomposite coatings had higher impedance values in the high frequency,

Table I. Polarization and Impendence Data Obtained from Tafel and Nyquist Plots

Sample	E_{corr}, V	$I_{corr} \times 10^{-6}$, Acm^{-2}	Corrosion rate mpy $\times 10^{-2}$	R_{ct}, Ω cm^2	C_{dl}, $\times 10^{-9}$ F/cm^2
316L	−0.443	34.71	130.00	504	185.81
TiN	−0.355	14.81	85.50	1077	81.22
Si_3N_4	−0.315	4.57	17.14	2719	9.13
Ti–Si–N	−0.182	0.38	1.45	13846	1.05

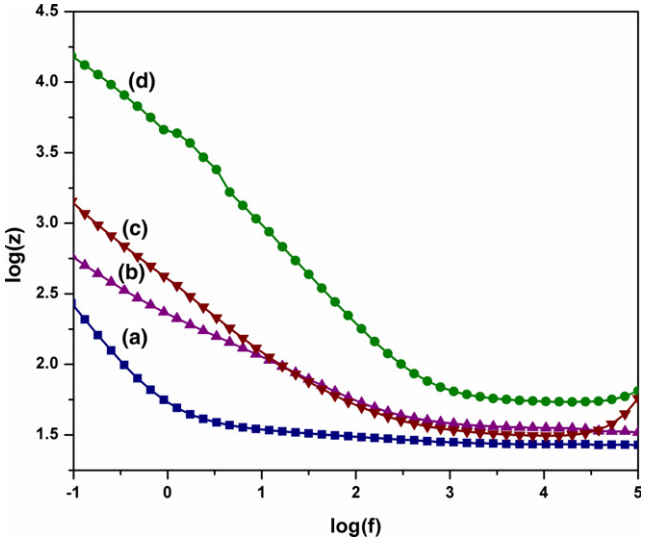

Fig. 7. Bode plot for (a) 316L, (b) TiN, (c) Si_3N_4, and (d) Ti–Si–N coatings in SBF solution.

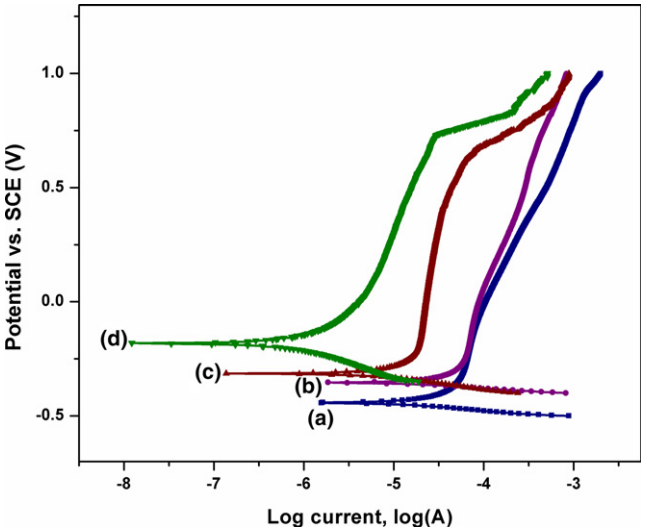

Fig. 8. Potentiodynamic polarization curve for (a) 316L, (b) TiN, (c) Si_3N_4, and (d) Ti–Si–N coatings in SBF solution.

indicating the good protective effectiveness of the coating. In contrast, the total impedance of single-layered TiN and Si_3N_4 coatings markedly changed with prolonged exposure to physiological solution due to degradation of the coating owing to pitting.

Typical potentiodynamic polarization curves of the coatings in deaerated SBF at 37°C are shown in Fig. 9. It can be seen that the polarization curve for Ti–Si–N nanocomposite samples had a significantly higher corrosion potential (−0.182 V) than that for samples (−0.355 V for TiN and −0.315 V for Si_3N_4). The results confirmed that nanocomposite Ti–Si–N coatings exhibited a better electrochemical behavior than TiN and Si_3N_4 coatings by virtue of more noble corrosion potential, although both the curves were characterized by a very similar trend. The corrosion current density and polarization resistance (R_p) of the specimens were determined from the potentiodynamic polarization curves using Tafel extrapolation method. The polarization resistance is a parameter correlated with the corrosion rate. The higher the polarization resistance, the lower the corrosion rate of the coating when exposed to SBF.[35] Table I indicates that the nanocomposite coatings had a lower current density compared with TiN and Si_3N_4 coatings.

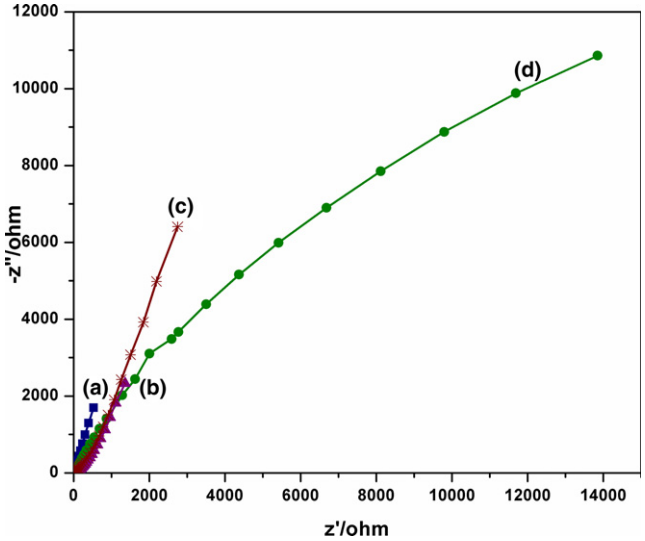

Fig. 9. Nyquist plot for (a) 316L, (b) TiN, (c) Si_3N_4, and (d) Ti–Si–N coatings in SBF solution.

From polarization test results, the protective efficiency, P_i (%) of the coatings can be calculated by Eq. (1):

$$P_i(\%) = \left[1 - \left(\frac{i_{corr}}{i^0_{corr}}\right)\right] \times 100 \quad (1)$$

where i_{corr} and i_{0corr} indicate the corrosion current density of the coating and substrate, respectively.[36] The protective ability of the coating increased with the incorporation of Si into the TiN coating. The Ti-Si-N coating showed the highest protective efficiency of 92.14% caused by the lowest corrosion current density of 0.38 μA/cm^2.

The *in vitro* electrochemical polarization corrosion test results indicated that the nanocomposite coatings had a more beneficial and desired effect on corrosion behavior than single layered samples; this was in accordance with the results from EIS.

IV. Conclusions

Ti–Si–N nanocomposite coatings were prepared by reactive dc magnetron sputtering onto 316L stainless steel substrates. XRD and XPS reveal that the hardest Ti–Si–N nanocomposite coating consists of fine TiN crystallites in an amorphous Si_3N_4 matrix. Preferential growth of TiN is indicated by TEM-SAED and XRD patterns. Lower surface roughness was observed for the Ti–Si–N coating layer when compared with the single-layer coating. The nanocomposite coatings showed the maximum hardness of 39 GPa. The potentiodynamic polarization and EIS measurements showed that the Ti–Si–N nanocomposite coatings exhibited superior corrosion resistance when compared with the SiN, TiN single layer, and the bare 316L SS substrate in simulated body fluid solution.

Acknowledgments

B.S, one of the authors, thanks the Department of Science & Technology, New Delhi, for a research grant under SERC scheme No SR/S1/PC/31/2008, and the Japan Society for the Promotion of Science, Japan for the award of FY 2011 JSPS Long term Invitation fellowship. We thank Prof M. Takahashi and Prof H. Nishikawa of Osaka University, Japan for the TEM and nanoindentation analyses.

References

[1]S. K. Tiwari, T. Mishra, M. K. Gunjan, A. S. Bhattacharyya, T. B. Singh, and R. Singh, "Development and Characterization of sol–Gel Silica–Alumina

Composite Coatings on AISI 316L for Implant Applications," *Surf. Coat. Technol.*, **201**, 7582–8 (2007).
[2]S. P. Patterson, R. H. Daffner, and R. A. Gallo, "Electrochemical Corrosion of Metal Implants," *AJR Am. J. Roentgenol.*, **184**, 1219–22 (2005).
[3]E. Ingham and J. Fisher, "Biological Reaction to Wear Debris in Total Joint Replacement," *Proc. Inst. Mech. Eng. H*, **214**, 21–37 (2000).
[4]R. F. Zhang, A. S. Argon, and S. Veprek, "Electronic Structure, Stability, and Mechanism of the Decohesion and Shear of Interfaces in Superhard Nanocomposites and Heterostructures," *Phys. Rev. B*, **79**, 245426–38 (2009).
[5]D. B. Lee, M. H. Kim, Y. C. Lee, and S. C. Kwon, "High Temperature Oxidation of TiCrN Coatings Deposited on a Steel Substrate by Ion Plating," *Surf. Coat. Technol.*, **141**, 232–9 (2001).
[6]S. M. Yang, Y. Y. Chang, D. Y. Wang, D. Y. Lin, and W. T. Wu, "Mechanical Properties of Nano-Structured Ti-Si-N Films Synthesized by Cathodic Arc Evaporation," *J. Alloys Compd.*, **440**, 375–9 (2007).
[7]J. D. Bressan, R. Hesse, and E. M. Silva Jr., "Abrasive Wear Behavior of High Speed Steel and Hard Metal Coated with TiAlN and TiCN," *Wear*, **250**, 561–8 (2001).
[8]S. H. Kim, J. W. Jang, S. S. Kang, and K. H. Kim, "Synthesis and Mechanical Evaluation of Nanocomposite Coating Layer of nc-TiN/a-Si_3N_4 on SKD 11 Steel by Sputtering," *J. Mater. Proc. Technol.*, **130–131**, 283–8 (2002).
[9]S. H. Kim, J. K. Kim, and K. H. Kim, "Influence of Deposition Conditions on the Microstructure and Mechanical Properties of Ti–Si–N Films by DC Reactive Magnetron Sputtering," *Thin Solid Films*, **420–421**, 360–5 (2002).
[10]F. Tang, B. Gault, S. P. Ringer, P. Martin, A. Bendavid, and J. M. Cairney, "Microstructural Investigation of Ti–Si–N Hard Coatings," *Scr. Mater.*, **63**, 192–5 (2010).
[11]A. Bendavid, P. J. Martin, E. W. Preston, J. Cairney, Z. H. Xie, and M. Hoffman, "Deposition of Nanocomposite Thin Films by a Hybrid Cathodic Arc and Chemical Vapour Technique," *Surf. Coat. Technol.*, **201**, 4139 (2006).
[12]P. J. Martin and A. Bendavid, "Properties of $Ti_{1-x}Si_xN_y$ Films Deposited by Concurrent Cathodic Arc Evaporation and Magnetron Sputtering," *Surf. Coat. Technol.*, **163–164**, 245–50 (2003).
[13]C. H. Zhang, Z. J. Liu, K. Y. Li, Y. G. Shen, and J. B. Luo, "Microstructure, Surface Morphology, and Mechanical Properties of Nanocrystalline TiN/Amorphous Si_3N_4 Composite Films Synthesized by Ion Beam Assisted Deposition," *J. Appl. Phys.*, **95**, 1460–7 (2004).
[14]S. Carvalho, L. Rebouta, E. Ribeiro, F. Vaz, M. F. Denannot, J. Pacaud, J. P. Rivière, F. Paumier, R. J. Gaboriaud, and E. Alves, "Microstructure of (Ti,Si,Al)N Nanocomposite Coatings," *Surf. Coat. Technol.*, **177–178**, 369–75 (2004).
[15]S. R. Choi, I. W. Park, J. H. Park, and K. H. Kim, "Influence of Substrate Bias Voltage on Deposition Behavior and Micro-Indentation Hardness of Ti–Si–N Coatings by a Hybrid Coating System of Arc Ion Plating and Sputtering Techniques," *Surf. Coat. Technol.*, **179**, 89–94 (2004).
[16]G. Lia, M. Mori, S. Miyake, M. Kumagai, H. Saito, and Y. Muramatsu, "Structure and Properties of Ti–Si–N Films Prepared by ICP Assisted Magnetron Sputtering," *Surf. Coat. Technol.*, **193**, 345–9 (2005).
[17]H. H. Huang, C. H. Hsu, S. J. Pan, J. L. He, C. H. Chen, and T. L. Lee, "Corrosion and Cell Adhesion Behavior of TiN-Coated and Ion-Nitrided Titanium for Dental Applications," *Appl. Surf. Sci.*, **244**, 252–6 (2005).
[18]Y. H. Cheng, T. Browne, and B. Heckerman, "Nanocomposite TiSiN Coatings Deposited by Large Area filtered Arc Deposition," *J. Vac. Sci. Technol. A*, **27** [1] 82–8 (2009).
[19]B. Subramanian, R. Ananthakumar, V. S. Vidhya, and M. Jayachandran, "Influence of Substrate Temperature on the Materials Properties of Reactive DC Magnetron Sputtered Ti/TiN Multilayered Thin Films," *Mater. Sci. Eng. B*, **176**, 1–7 (2011).
[20]Z. T. Yang, B. Yang, L. P. Guo, and D. J. Fu, "Synthesis of Ti-Si-N Nanocomposite Coatings by a Novel Cathodic Arc Assisted Middle-Frequency Magnetron Sputtering," *Appl. Surf. Sci.*, **255**, 4720–4 (2009).
[21]C. W. Zou, H. J. Wang, M. Li, Y. F. Yu, C. S. Liu, L. P. Guo, and D. J. Fu, "Characterization and Properties of TiN-Containing Amorphous Ti-Si-N Nanocomposite Coatings Prepared by Arc Assisted Middle Frequency Magnetron Sputtering," *Vacuum*, **84**, 817–22 (2010).
[22]J. F. Marco, A. C. Agudelo, J. R. Gancedo, and D. Hanzel, "Corrosion Resistance of Single TiN Layers, Ti/TiN Bilayers and Ti/TiN/Ti/TiN Multilayers on Iron Under a Salt fog Spray (Phohesion) Test: An Evaluation by XPS," *Surf. Interface Anal.*, **27**, 71–5 (1999).
[23]T. Choudhury, S. O. Saied, and J. L. Sullivan, "Reduction of Oxides of Iron, Cobalt, Titanium and Niobium by Low-Energy Ion Bombardment," *J. Phys. D*, **22**, 1185–95 (1989).
[24]M. Balaceanu, M. Braic, D. Macovei, M. J. Genet, A. Manea, D. Pantelica, V. Braic, and F. Negoita, "Properties of Titanium Based Hard Coatings Deposited by the Cathodic Arc Method i. Microchemical and Microstructural Characteristics," *J. Optoelectron. Adv. Mater.*, **4**, 107–14 (2002).
[25]P. Padmavathy, R. Ananthakumar, B. Subramanian, C. Ravidhas, and M. Jayachandran, "Structural and Electrochemical Impedance Spectroscopic Studies on Reactive Magnetron Sputtered Titanium Oxynitride (TiON) Thin Films," *J. Appl. Electrochem.*, **41**, 751–6 (2011).
[26]H. C. Barshilia, B. Deepthi, A. S. Arun Prabhu, and K. S. Rajam, "Superhard Nanocomposite Coatings of TiN/Si_3N_4 Prepared by Reactive Direct Current Unbalanced Magnetron Sputtering," *Surf. Coat. Technol.*, **201**, 329–37 (2006).
[27]H. Mu, J. Seok, and R. Y. Lin, "Nickel Thin Film Coatings on Steels with Electroless Plating and Sputter Deposition," *J. Electrochem. Soc.*, **150** [2] c67–72 (2003).
[28]Y. C. Ee, Z. Chen, S. Xu, L. Chan, K. H. See, and S. B. Law, "Electroless Copper Deposition as a Seed Layer on TiSiN Barrier," *J. Vac. Sci.Technol. A*, **22**, 1852–6 (2004).
[29]M. Shinn and S. A. Bannett, "Growth, Structure, and Microhardness of Epitaxial TiN/NbN Superlattices," *J. Mater. Res.*, **7**, 901–11 (1992).
[30]A. H. Cottrell, *An Introduction to Metallurgy*, p. 394, Edward Arnold, London, 1967.
[31]G. S. Kim, B. S. Kim, S. Y. Lee, and J. H. Hahn, "Effect of Si Content on the Properties of TiAl–Si–N Films Deposited by Closed Field Unbalanced Magnetron Sputtering with Vertical Magnetron Sources," *Thin Solid Films*, **506–507**, 128–32 (2006).
[32]M. Diserens, J. Patscheider, and F. Levy, "Improving the Properties of Titanium Nitride by Incorporation of Silicon," *Surf. Coat. Technol.*, **108–109**, 241–6 (1998).
[33]S. R. Paital, and N. B. Dahotre, "Calcium Phosphate Coatings for Bio-Implant Applications: Materials, Performance Factors, and Methodologies," *Mater. Sci. Eng: R Rep.*, **66**, 1–70 (2009).
[34]C. Liu, Q. Bi, and A. Mathews, "EIS Comparison on Corrosion Performance of PVD TiN and CrN Coated Mild Steel in 0.5 N NaCl Aqueous Solution," *Corr. Sci.*, **43**, 1953–61 (2001).
[35]T. M. Sridhar, U. K. Mudali, and M. Subbaiyan, "Preparation and Characterisation of Hydroxya-Patite Coated 316L Stainless Steel," *Corros. Sci.*, **45**, 237–52 (2003).
[36]Y. H. Yoo, D. P. Le, J. G. Kim, S. K. Kim, and P. V. Vinh, "Corrosion Behavior of TiN, TiAlN, TiAlSiN Thin Films Deposited on Tool Steel in the 3.5 wt.% NaCl Solution," *Thin Solid Films* **516**, 3544–8 (2008). □